FEBRUARY 06 2024

# Effects of viscous dissipation in propagation of sound in periodic layered structures

Dmitrii Shymkiv; Arkadii Krokhin



*J. Acoust. Soc. Am.* 155, 990–1004 (2024)
https://doi.org/10.1121/10.0024719

JASA ARTICLE

# Effects of viscous dissipation in propagation of sound in periodic layered structures

Dmitrii Shymkiv and Arkadii Krokhin[a)]
*Department of Physics, University of North Texas, Denton, Texas 76203, USA*

**ABSTRACT:**
Propagation and attenuation of sound through a layered phononic crystal with viscous constituents is theoretically studied. The Navier–Stokes equation with appropriate boundary conditions is solved and the dispersion relation for sound is obtained for a periodic layered heterogeneous structure where at least one of the constituents is a viscous fluid. Simplified dispersion equations are obtained when the other component of the unit is either elastic solid, viscous fluid, or ideal fluid. The limit of low frequencies when periodic structure homogenizes and the frequencies close to the band edge when propagating Bloch wave becomes a standing wave are considered and enhanced viscous dissipation is calculated. Angular dependence of the attenuation coefficient is analyzed. It is shown that transition from dissipation in the bulk to dissipation in a narrow boundary layer occurs in the region of angles close to normal incidence. Enormously high dissipation is predicted for solid–fluid structure in the region of angles where transmission practically vanishes due to appearance of so-called "transmission zeros," according to El Hassouani, El Boudouti, Djafari-Rouhani, and Aynaou [Phys. Rev. B **78**, 174306 (2008)]. For the case when the unit cell contains a narrow layer of high viscosity fluid, the anomaly related to acoustic manifestation of Borrmann effect is explained.
 https://doi.org/10.1121/10.0024719

(Received 13 October 2023; revised 9 January 2024; accepted 17 January 2024; published online 6 February 2024)

[Editor: Likun Zhang] Pages: 990–1004



## I. INTRODUCTION

Acoustic properties of layered elastic structures have been a subject of active research for more than a century. Combining layers of different widths and of different elastic materials, a wide variety of elastic properties can be tailored, which makes these structures applicable in many areas of modern technology.[1] Quite a full collection of acoustic and elastic properties of layered structures can be found in two fundamental books.[2,3]

A special case of layered media is a medium with spatial periodicity, i.e., elastic superlattice or one-dimensional (1D) phononic crystal. Due to additional symmetry related to periodicity, mathematical theory of wave propagation in superlattices has been strongly advanced. In particular, the dispersion relation between the Bloch vector $\mathbf{k}$ and frequency $\omega$ has been derived in analytical form.[4] If the constituents are dissipative, the dispersion relation $\omega = \omega(\mathbf{k})$ becomes complex and the oscillations of acoustic pressure decays exponentially with distance, even for the frequency lying within a propagating band. A phenomenological method to introduce dissipation is to add imaginary parts to the elastic constants.[5,6] Since dissipation vanishes in static limit, the imaginary additions are linear over $\omega$ (viscous friction), which enhances the effect of dissipation on dispersion of sound.[7–9]

If at least one of the constituents of phononic crystal is a viscous fluid, a microscopic description of fluid dynamics in acoustic field becomes possible through the Navier–Stokes equation. As compared to bulk losses, viscous friction is much stronger near a fluid–solid interface due to formation of a narrow boundary layer $\delta$, where the tangential component of velocity of oscillating fluid, $\mathbf{v}(x,t)$ decays exponentially towards the interface with distance $x$, $v(x,t) \sim (1 - e^{-x/\delta})\ e^{-i\omega t}$. Dissipated power depends on velocity gradients $(\partial v_i/\partial x_j)^2$. Since the width of the boundary layer is usually much less than the wavelength $\lambda$, the viscous losses in the bulk can be neglected as compared to the losses within the layer $\delta$. The bulk losses grow as $\eta\omega^2$ and the boundary layer losses grow as $\sqrt{\omega\eta}$, where $\eta$ is the shear viscosity coefficient. At low frequencies, this essential difference gives rise to so-called Konstantinov's effect, which predicts enhanced absorption at reflection of sound from a fluid–solid interface.[10]

Due to Konstantinov's effect, acoustic absorption in a fluid–solid phononic crystal is strongly inhomogeneous and its calculation requires solution of the linearized Navier–Stokes equation and continuity equation. Mathematical analysis made on the basis of linearized Navier–Stokes equation shows that some effects originated from fluid viscosity and lack of inverse symmetry in periodic two-dimensional (2D) and three-dimensional (3D) elastic structures cannot be fully described by the wave equation for inviscid fluid where elastic modulus and fluid density acquire phenomenological imaginary additions.[11] The phenomenological Rayleigh damping model,[9,12] widely used in seismology and architecture,[13] is also unable to correctly account for enhanced viscous dissipation within the boundary layer. Strongly

a)Email: arkadii.krokhin@unt.edu

 

https://doi.org/10.1121/10.0024719

inhomogeneous distribution of fluid velocities gives rise to spatial dispersion of the dissipative terms in the wave equation, which depend not only on $\omega$, but also on $\mathbf{k}$. Moreover, formation of the viscous boundary layer and dissipated power depend on the shape of solid inclusions. In particular, presence of sharp corners, where velocity gradients and local dissipated power become very high, is ignored in the phenomenological approach. The phenomenological approach can be improved[14] by adopting some results from the acoustics of porous medium, in particular, by accounting for the effects of the viscous boundary layer in the imaginary parts of effective mass density and effective elastic moduli.

The microscopic approach based on the Navier–Stokes dynamical equation accounts for formation of a highly dissipative boundary layer around each scatterer as well as for viscous dissipation in the bulk. The wave equation for sound in a viscous environment with shear and bulk viscosity coefficients can be formally reduced to the wave equation in a dissipationless isotropic solid with complex frequency-dependent Lamé coefficients, which are microscopically justified.[15]

Scattering of sound by solid inclusions of different shape embedded in a viscous fluid has a long history, starting from the pioneering works by Sewell[16] and Lamb.[17] We refer here to a relatively modern study[18] where the Navier–Stokes equation is used for analytical calculations of the scattering cross section, acoustic-radiation force, and attenuation coefficient for an elastic sphere and cylinder in a viscous background. The field of fluid velocities was represented as a superposition of two components: acoustic potential wave and vortex shear wave.[19] The influence of viscosity on the scattering pattern produced by a single scatterer turns out to be quite low.[18] However, multiple scattering and interference strongly enhance viscous and thermal losses for sound propagating in a phononic crystal, especially at high filling fractions when the boundary layers of the neighbouring scatterers start to overlap.[14,20–24] In the long-wavelength limit, phononic crystal behaves like a homogeneous metamaterial where effective viscosity may exhibit strong anisotropy,[23,24] together with elastic moduli, mass density, and speed of sound.

This paper addresses sound propagation through a periodic layered structure containing viscous fluid constituents. We develop a microscopic theory based on Navier–Stokes equation. While the analytical calculations are cumbersome, it is possible to reduce the dispersion equation to the form similar to that derived by Rytov.[4] The obtained dispersion equation gives in implicit form the relation $f(\omega, \mathbf{k}) = 0$ for any frequency and direction of propagation. At finite viscosity, the solutions $\mathbf{k} = \mathbf{k}(\omega)$ of the dispersion equation are complex; $\mathbf{k} = \mathbf{k}'(\omega) + i\mathbf{k}''(\omega)$ at any frequency $\omega$. Analyzing the dispersion relation in the long-wavelength limit, we obtain analytical expression for the attenuation coefficient $k''(\omega)$, which exhibits very strong uniaxial anisotropy. Namely, the frequency dependence $k''(\omega)$ turns out to be different for oblique and normal incidence of sound. We explain a transition from $\omega^2$ dependence of dissipated power to $\sqrt{\omega}$ law when the direction of propagation slightly deviates from propagation parallel to the superlattice axis. The effective viscosity as a frequency-independent parameter can be introduced in the long-wavelength limit for normal incidence only. Viscous losses are analyzed in the vicinity of the band gaps, where group velocity vanishes, which leads to a strong increase in dissipation. If one of the fluids is viscous and another is inviscid, the low-frequency expansion of $k''(\omega)$ starts from the terms higher than $\sqrt{\omega}$, i.e., the Konstantinov's effect is suppressed since there is no viscous friction at the interface. There is an interesting opposite case of a very viscous but narrow layer in contact with a layer of ideal (inviscid) fluid. For this combination of materials, an acoustic analog of so-called Borrmann effect is predicted when, for certain frequencies, the transmission becomes anomalously high. At these frequencies, the nodes of fluid velocity lie inside the viscous layers, which strongly reduces viscous losses.

While the proposed theory is based on the microscopic, not a phenomenological approach, it remains a classical macroscopic hydrodynamic theory in the sense that the thickness of the fluid layers contains many atomic spacings. The atomic structure becomes important in consideration of hydrodynamics of nanofluids (lubricants), when the direct interactions between atomically flat solid surface and atomically thin liquid layer contribute to the friction forces. The classical no-slip boundary condition is violated in this case due to arrangement of the molecules of liquid into layers parallel to solid surfaces[25] and the effective viscosity strongly exceeds its classical macroscopic value.[26] Intermolecular interactions not only enhance classical friction forces but also make the dependence on the discrete thickness of the stacked sheets of atoms a discontinuous function.[27] A similar situation occurred in 1947 with the theory of anomalous skin-effect in metals. The "noneffectiveness concept" proposed by Pippard,[28] being phenomenological, explained the physical nature of the effect and most of the experimental results for surface impedance. One year later, a microscopic theory based on the kinetic equation for conduction electrons was developed by Reuter and Sondheimer.[29] Both theories are classical, but the microscopic theory is more complete, explaining some fine details related to electron scattering at rough metal surfaces.

## II. TWO EIGEN MODES IN FREE VISCOUS FLUID

A monochromatic acoustic wave propagating in a viscous fluid excites oscillations with frequency $\omega$. Distribution of fluid velocities $\mathbf{v}(\mathbf{r})e^{-i\omega t}$ satisfies the wave equation

$$\rho\omega^2 v_i + \lambda \frac{\partial}{\partial x_i}(\nabla \cdot \mathbf{v}) = i\omega\eta \frac{\partial}{\partial x_k}\left(\frac{\partial v_i}{\partial x_k} + \frac{\partial v_k}{\partial x_i} - \frac{2}{3}\delta_{ik}\nabla \cdot \mathbf{v}\right) + i\omega\xi \frac{\partial}{\partial x_i}(\nabla \cdot \mathbf{v}), \quad (1)$$

which is obtained from the linearized Navier–Stokes equation and continuity equation. Here, $\rho$ is the fluid density, $\lambda$ is the bulk elastic modulus, and $\eta$ and $\xi$ are the shear and bulk viscosity coefficients.

In a homogeneous infinite fluid, the solutions of Eq. (1) can be written in a form of a plane wave

$$\mathbf{v}(\mathbf{r}) = \mathbf{V}e^{i\mathbf{k}\cdot\mathbf{r}}. \tag{2}$$

Velocity amplitude $\mathbf{V}$ satisfies the following linear equation:

$$\left(\omega^2 + i\omega\frac{\eta}{\rho}k^2\right)\mathbf{V} = \left(c^2 - \frac{1}{3\rho}i\omega\eta - i\omega\frac{\xi}{\rho}\right)(\mathbf{k}\cdot\mathbf{V})\mathbf{k}, \tag{3}$$

where $c^2 = \lambda/\rho$. There are two eigenmodes with different polarizations and dispersions obtained from Eq. (3):

*Longitudinal polarization*, $\mathbf{V}||\mathbf{k}$,

$$k_l^2 = \frac{\omega^2/c^2}{1 - \frac{i\omega}{\rho c^2}\left(\frac{4}{3}\eta + \xi\right)} \tag{4}$$

*Transverse polarization*, $\mathbf{V}\perp\mathbf{k}$,

$$k_t^2 = \frac{i\omega\rho}{\eta} = \frac{2i}{\delta^2}, \quad \delta = \sqrt{\frac{2\eta}{\omega\rho}}. \tag{5}$$

Dispersion relations [Eqs. (4) and (5)] involve complex wave vector

$$\mathbf{k} = k'\mathbf{n} + ik''\mathbf{a}, \tag{6}$$

where $\mathbf{n}$ and $\mathbf{a}$ are the propagation and attenuation unit vectors, respectively. Generally, these vectors are not parallel but make an angle $\gamma$ with each other. A plane wave with a complex wave vector is a so-called inhomogeneous plane wave where $\gamma$ is the degree of inhomogeneity.[30] The real and imaginary parts of the wave vector are expressed through $R = \mathrm{Re}(k^2)$ and $I = \mathrm{Im}(k^2)$ as follows:

$$k'^2 = \frac{1}{2}\left(R + \sqrt{R^2 + \frac{I^2}{\cos^2\gamma}}\right),$$
$$k''^2 = \frac{1}{2}\left(-R + \sqrt{R^2 + \frac{I^2}{\cos^2\gamma}}\right). \tag{7}$$

Propagating sound wave is associated with the longitudinal mode. Long-distance propagation occurs if the attenuation factor $e^{-k_l''x}$ remains practically constant at the wavelength scale $2\pi/k_l' = 2\pi c/\omega$, which requires $I \ll R$, i.e.,

$$\frac{I}{R} = \frac{\omega}{\rho c^2}\left(\frac{4}{3}\eta + \xi\right) \approx \frac{\omega\eta}{\rho c^2} \ll 1. \tag{8}$$

Under this condition, expansion of $k_l''$ in Eq. (7) gives

$$k_l'' \approx \frac{I}{2\sqrt{R}\cos\gamma_l} = k_l'\frac{\omega}{2\rho c^2\cos\gamma_l}\left(\frac{4}{3}\eta + \xi\right) \ll k_l'. \tag{9}$$

Here, $k_l''$ is the bulk attenuation coefficient of sound wave representing exponential decay $\sim e^{-k_l''x}$ of the wave amplitude with distance due to viscous dissipation. Inequality [Eq. (9)] defines a wideband of frequencies

$$\omega \ll \omega^\star = \rho c^2/\eta, \tag{10}$$

where attenuation of sound due to dissipative losses remains small. For example, in water, sound does not suffer from strong viscous attenuation for frequencies below 1 THz.

The transverse mode where $R = 0$ is not a propagating wave. If excited, it decays within the distance $\delta = \sqrt{2\eta/\rho\omega}$, which coincides with the viscous boundary layer thickness

$$k_t' = k_t'' = 1/\delta\sqrt{\cos\gamma_t}. \tag{11}$$

This mode is a hydrodynamic analog of electromagnetic wave penetrating inside a metal surface. Due to high conductivity of metal, electromagnetic wave decays within the skin layer. In both cases, the fields decay exponentially (normal skin-effect) and the thickness of the boundary (or skin) layer decreases with frequency as $\omega^{-1/2}$. In an infinite fluid without scatterers, the two modes are decoupled and isotropy requires that angle $\gamma = 0$. At any interface, the modes coupling occurs through the non-slip boundary condition for velocity. Due to this coupling, the acoustic viscous losses grow by orders of magnitude as compared to free fluid.[10]

Phase velocities and attenuations of the longitudinal and transverse modes satisfy the inequality[31]

$$\frac{k_l''}{k_l'(1 + k_l''^2/k_l'^2)^2} > \frac{4c_t^2}{3c_l^2}\frac{k_t''}{k_t'(1 + k_t''^2/k_t'^2)^2}. \tag{12}$$

For the longitudinal mode $k_l'' \ll k_l'$ and $c_l = c = \omega/k_l'$. For the evanescent transverse mode, $k_t'' = k_t'$ and $c_t = \omega/k_t' = \omega\delta$. It is easy to see that in a viscous fluid, the inequality [Eq. (12)] is reduced to $\xi/\rho > 0$, which is obviously satisfied.

## III. DISPERSION EQUATION FOR SOUND WAVE IN A SUPERLATTICE WITH VISCOUS CONSTITUENTS

We consider a binary periodic structure consisting of parallel layers. The unit cell of length $d = a + b$ is shown in Fig. 1. The layer $a$ is a viscous fluid. In the general case, the layer $b$ is an elastic solid. Manipulating with its elastic moduli, the particular cases of ideal or viscous fluid can be analyzed as well.

### A. Solution of the wave equation

In the presence of boundaries, the solution of the wave [Eq. (1)] is written as a sum of longitudinal (potential) and transverse (solenoidal) mode

https://doi.org/10.1121/10.0024719

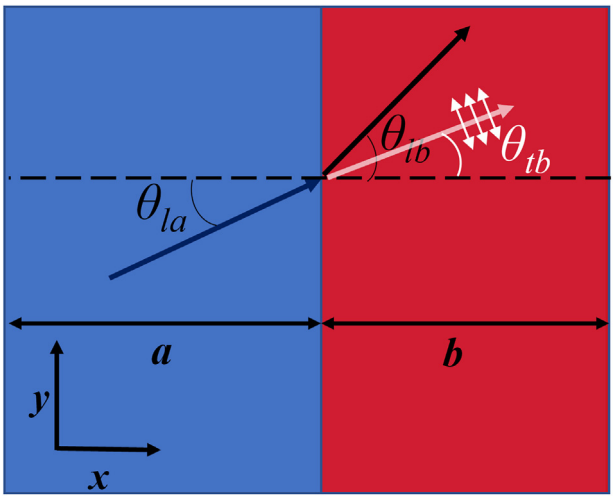


FIG. 1. (Color online) Unit cell of elastic superlattice with period $d = a + b$ consisting of two layers: viscous fluid $a$ and elastic solid $b$. Arrows show the incident longitudinal mode in fluid and two (longitudinal and transverse) refracted modes in solid.

$$\mathbf{v}(\mathbf{r}) = \mathbf{v}_l(\mathbf{r}) + \mathbf{v}_t(\mathbf{r}). \tag{13}$$

It follows from the structure of the solutions of Eq. (3) that the longitudinal mode is potential, $\mathbf{v}_l = \nabla\phi$, and the transverse mode is solenoidal, $\mathbf{v}_t = \nabla \times \mathbf{A}$, where $\mathbf{A} = (0, 0, A_z)$. Each potential satisfies the wave equation with the corresponding speed of sound, $\omega/k_l$ and $\omega/k_t$. In the solid layer, the speeds are real. In the fluid layer, both speeds are complex according to Eqs. (4) and (5). The solutions of the wave equations for the potentials are represented by superpositions of plane waves travelling along and against axis $x$.

Scattering at the vertical boundary does not change the $y$-component of the complex wave vector of each mode, $k^{(a)}_{(l,t)y} = k^{(b)}_{(l,t)y}$. Within each layer, the velocities $\mathbf{v}_l$ and $\mathbf{v}_t$ are obtained by differentiating the corresponding potentials. For the longitudinal mode, the terms representing plane waves travelling along and against axis $x$ enter with the same sign to the $y$ component of velocity, $v_{yl} = \partial\phi/\partial y$, and with the opposite signs to the $x$ component, $v_{xl} = \partial\phi/\partial x$. The general solution for the velocity in the longitudinal mode can be written as follows:

$$\mathbf{v}_l(\mathbf{r}) = (\mathbf{n}_l + i\epsilon\mathbf{a}_l)\Big[Ae^{k'_l x(i\cos\theta_l - \epsilon\cos(\theta_l-\gamma_l))} \mp Be^{-k'_l x(i\cos\theta_l - \epsilon\cos(\theta_l-\gamma_l))}\Big] e^{k'_l y(i\sin\theta_l - \epsilon\sin(\theta_l-\gamma_l))}, \tag{14}$$

where the minus (plus) sign is selected for the $x$ ($y$) component. Here, the small parameter $\epsilon = k''_l/k'_l = (4/3\eta + \xi)\omega/(2\rho c^2\cos\gamma_l) \sim \omega^\star/\omega \ll 1$ defines the attenuation rate. Angles $\theta_l$ and $\gamma_l$ give the directions of the unit vectors $\mathbf{n}_l = (\cos\theta_l, \sin\theta_l)$ and $\mathbf{a}_l = (\cos(\theta_l - \gamma_l), \sin(\theta_l - \gamma_l))$.

The transverse mode has two polarizations in the "plane" perpendicular to the wave vector $\mathbf{k}_t$, i.e., to $\mathbf{n}_t + i\mathbf{a}_t$, where $\mathbf{n}_t = (\cos\theta_t, \sin\theta_t)$ and $\mathbf{a}_t = (\cos(\theta_t - \gamma_t), \sin(\theta_t - \gamma_t))$. Any two non-collinear vectors lying in this "plane" may serve as polarization vectors, for example, the vectors $\hat{\mathbf{z}} \times (\mathbf{n}_t + i\mathbf{a}_t) = (-n_{ty} - ia_{ty}, n_{tx} + ia_{tx})$ and $\hat{\mathbf{z}} \times (-\mathbf{a}_t + i\mathbf{n}_t) = (a_{ty} - in_{ty}, -a_{tx} + in_{tx})$. Using the former vector, the solution for the transverse mode is written as follows:

$$\mathbf{v}_\mathbf{t} = \hat{\mathbf{z}} \times (\mathbf{n}_t + i\mathbf{a}_t)\Big[Ce^{(x/\delta\sqrt{\cos\gamma_t})(i\cos\theta_t - \cos(\theta_t-\gamma_t))} \pm De^{-(x/\delta\sqrt{\cos\gamma_t})(i\cos\theta_t - \cos(\theta_t-\gamma_t))}\Big] \times e^{(y/\delta\sqrt{\cos\gamma_t})(i\sin\theta_t - \sin(\theta_t-\gamma_t))}, \tag{15}$$

where plus (minis) sign is selected for $v_{xt} = \partial A_z/\partial y$ ($v_{yt} = -\partial A_z/\partial x$).

### B. Refraction at the interface and generalized Snell's law

Refraction at the boundary between the layer $a$ of viscous fluid and the layer $b$ of elastic solid (Fig. 1) leads to the coupling among the longitudinal and transverse modes in the fluid and solid. All four modes propagate with equal $y$-component of the wave vector, $k_{ly} = k_{ty}$. Since these $y$-components conserve at refraction/reflection, the Snell's law generalized for an inhomogeneous wave is written as follows:

$$\frac{\omega}{c_a}[\sin\theta_{la} + i\epsilon_a\sin(\theta_{la} - \gamma_{la})] = \frac{\sin\theta_{ta} + i\sin(\theta_{ta} - \gamma_{ta})}{\delta_a\sqrt{\cos\gamma_{ta}}} = \frac{\omega}{c_{lb}}\sin\theta_{lb} = \frac{\omega}{c_{tb}}\sin\theta_{tb}. \tag{16}$$

Here, $c_{lb(tb)}$ is speed of longitudinal (transverse) mode in solid. The set of equations in Eq. (16) describes several interesting effects related to mutual transformations from longitudinal to transverse sound and the Fano resonances associated with multiple reflections and refractions. These effects were studied in detail in Refs. 3, 32, and 33. Here, we are interested in calculation of acoustic energy dissipated in the fluid $a$.

The real part of Eq. (16) yields

$$\frac{\omega}{c_a}\sin\theta_{la} = \frac{\omega}{c_{lb}}\sin\theta_{lb} = \frac{\omega}{c_{tb}}\sin\theta_{tb} = \frac{\sin\theta_{ta}}{\delta_a\sqrt{\cos\gamma_{ta}}}. \tag{17}$$

The first and second equality are the Snell's law for the longitudinal-to-longitudinal refraction, $\sin\theta_{la}/\sin\theta_{lb} = c_a/c_b$, and for the longitudinal-to-transverse refraction, $\sin\theta_{la}/\sin\theta_{tb} = c_a/c_{tb}$. The equality $(\omega/c_a)\sin\theta_{la} = (\sin\theta_{ta}/\delta_a\sqrt{\cos\gamma_{ta}})$ means that $\sin\theta_{ta} \sim \delta_a(\omega/c_a) = k'_{la}\delta_a \ll 1$. Thus, due to low viscosity [see Eq. (8)], the transverse mode "propagates" almost perpendicular to the boundary and does not suffer from refraction. Note that this property is additional evidence that this mode is similar to the electromagnetic wave which for any angle of incidence "propagates" perpendicular to metal surface at a distance of the order of skin layer.

Separating the imaginary part of Eq. (16), one obtains the following relation for the angles $\theta_{ta}$ and $\gamma_{ta}$:

$$\frac{\epsilon_a\,\omega}{c_a}\sin(\theta_{la}-\gamma_{la})=\frac{\sin(\theta_{ta}-\gamma_{ta})}{\delta_a\sqrt{\cos\gamma_{ta}}}, \tag{18}$$

which assumes that the difference $\theta_{ta}-\gamma_{ta}$ is cubic over a small parameter $\epsilon_a\delta_a\omega/c_a\sim(k'_{la}\delta_a)^3$. Finally, the set of equations [Eq. (16)] can be written in a compact form

$$\frac{\sin\theta_{la}}{\sin\theta_{lb}}=\frac{c_a}{c_{lb}},\qquad \frac{\sin\theta_{la}}{\sin\theta_{tb}}=\frac{c_a}{c_{tb}},$$
$$\theta_{ta}=\gamma_{ta}=\frac{\omega\delta_a}{c_a}\sin\theta_{l(a)}\ll 1. \tag{19}$$

The relation between the angles $\theta_{la}$ and $\gamma_{la}$ depends on the initial conditions of excitation of sound and remains indefinite. This, however, does not affect further calculations since dissipation of the longitudinal mode gives negligible contribution to the attenuation of sound. The principal contribution comes from the transverse mode, which excites oscillations of fluid parallel to the interface at any direction of propagation of sound wave in the layered structure but the direction exactly parallel to the axis when $\theta_{ta}=\gamma_{ta}=0$.

### C. Boundary conditions at the interface

Within each layer, the velocities of the longitudinal and transverse mode are given by Eqs. (14) and (15), respectively. These equations contain four indefinite coefficients for each layer, i.e., in total there are eight unknowns. They are obtained from the boundary conditions at the interface $x=a$ (see Fig. 1). When sound wave passes through the interface, the oscillating total velocity in Eq. (13) satisfies the no-slip boundary condition, which means that $\mathbf{v}=\mathbf{v}_l+\mathbf{v}_t$ is continuous at $x=a$. Also, the normal, $F_x=\sigma_{xx}n_x$, and the tangential, $F_y=\sigma_{yx}n_x$, components of the force are continuous, which leads to continuity of the components $\sigma_{xx}$, $\sigma_{xy}$ of the stress tensor. Each continuity condition is supplemented by Floquet periodicity condition that relates the value at $x=0$ with the corresponding value at $x=a+b=d$. Eight boundary conditions can be written as follows:

$$\begin{aligned}
&v_{xa}(x=a)=v_{xb}(x=a),\\
&v_{ya}(x=a)=v_{yb}(x=a),\\
&e^{ik_xd}v_{xa}(x=0)=v_{xb}(x=a+b),\\
&e^{ik_xd}v_{ya}(x=0)=v_{yb}(x=a+b),\\
&\sigma^{(a)}_{xx}(x=a)=\sigma^{(b)}_{xx}(x=a),\\
&e^{ik_xd}\sigma^{(a)}_{xx}(x=0)=\sigma^{(b)}_{xx}(x=a+b),\\
&\sigma^{(a)}_{xy}(x=a)=\sigma^{(b)}_{xy}(x=a),\\
&e^{ik_xd}\sigma^{(a)}_{xy}(x=0)=\sigma^{(b)}_{xy}(x=a+b).
\end{aligned} \tag{20}$$

Here, $k_x$ is the $x$-component of the Bloch vector. In a linear medium, the components of the stress tensor are calculated through the total velocity [Eq. (13)]. For viscous fluid,

$$\sigma_{ik}=\frac{i}{\omega}\left(\lambda_f+\frac{2}{3}i\omega\eta-i\omega\xi\right)\delta_{ik}\nabla\cdot\mathbf{v}+\eta\left(\frac{\partial v_i}{\partial x_k}+\frac{\partial v_k}{\partial x_i}\right). \tag{21}$$

If one of the layers is elastic solid, the stress tensor is obtained from Eq. (21) by substitution

$$\lambda_f+\frac{2}{3}i\omega\eta-i\omega\xi\to\lambda_s,\qquad \eta\to\frac{i\mu_s}{\omega}, \tag{22}$$

where $\lambda_s$ and $\mu_s$ are the Lamé coefficients of the solid layer. Note that the stress tensor [Eq. (21)] and the relations [Eq. (22)] allow formal treatment of viscous fluid as elastic solid with complex Lamé coefficients. This analogy was explored in Ref. 15 for calculation of the contribution of surface degrees of freedom to the specific heat of a finite-size fluid sample and for band structure calculations of solid–viscous fluid phononic crystal.[20]

### D. Dispersion relation

Boundary conditions [Eq. (20)] form a set of homogeneous equations for eight unknown coefficients defining the velocity of the longitudinal [Eq. (14)] and transverse [Eq. (15)] mode over the unit cell. The dispersion relation $\omega=\omega(\mathbf{k})$ is obtained from the condition of vanishing of the determinant of this homogeneous set. The explicit form of the $8\times 8$ determinant is given in Appendix A.

Explicit calculation of the determinant leads to $8!=40,320$ terms in the dispersion equation. However, it can be essentially simplified in some particular cases and/or in the approximation of low viscosity. If sound wave propagates along the superlattice axis (normal incidence), the determinant factorises in two terms corresponding to the longitudinal and transverse mode. Only for this geometry, these two modes are decoupled, giving rise to the following two independent dispersion relations:

$$\cos(k_xd)=\cos(ak_a)\cos(bk_b)-\frac{1}{2}\left[\frac{k_a\rho_b}{k_b\rho_a}+\frac{k_b\rho_a}{k_a\rho_b}\right]\sin(ak_a)\sin(bk_b), \tag{23}$$

$$\cos(k_xd)=\cos(a\kappa_a)\cos(b\kappa_b)-\frac{1}{2}\left[\frac{\kappa_a\rho_b}{\kappa_b\rho_a}+\frac{\kappa_b\rho_a}{\kappa_a\rho_b}\right]\sin(a\kappa_a)\sin(b\kappa_b). \tag{24}$$

Here, $k_{a,b}(\kappa_{a,b})$ is the $x$-component of the longitudinal (transverse) mode in each layer.

$$k_{a,b}=\frac{\omega/c_{a,b}}{\sqrt{1-i\dfrac{\omega}{\rho_{a,b}c^2_{a,b}}\left(\dfrac{4}{3}\eta_{a,b}+\xi_{a,b}\right)}}, \tag{25}$$

$$\kappa_{a,b}=\sqrt{\frac{2i}{\delta_{a,b}}}. \tag{26}$$

https://doi.org/10.1121/10.0024719

If layer $b$ is an elastic dissipationless solid, then $k_b = \omega/c_l$, $\eta_b = \xi_b = 0$ and $\kappa_b = \omega/c_t$. Note that in the limit of weak attenuation, the imaginary part of $k_{a,b} \propto \omega^2$, which is a signature of pure bulk dissipation. The boundary layer is not formed at normal incidence.

Equations (23) and (24) have "standard" Rytov's form. Equation (24) provides dispersion for the transverse wave. It turns out to be almost a deaf mode since it cannot be excited at normal incidence if the wave source is in the far zone or if the environment outside the superlattice is an ideal fluid. The dispersion equations are exact over viscosity coefficients $\eta$ and $\xi$. In the most interesting case of low viscosity, the linear expansion of Eq. (23) gives the following result for the attenuation coefficient of the longitudinal wave:

$$k_x''(\omega)d = \frac{\omega^2}{2\sin(k_x'd)}\left\{\frac{\left(\frac{4}{3}\eta_a+\xi_a\right)a}{\rho_a c_a^3}\sin\left(\frac{\omega a}{c_a}\right)\cos\left(\frac{\omega b}{c_b}\right)+\frac{\left(\frac{4}{3}\eta_b+\xi_b\right)b}{\rho_b c_b^3}\sin\left(\frac{\omega b}{c_b}\right)\cos\left(\frac{\omega a}{c_a}\right)\right.$$
$$+\frac{1}{2\omega}\left(\frac{\frac{4}{3}\eta_a+\xi_a}{\rho_a c_a^2}-\frac{\frac{4}{3}\eta_b+\xi_b}{\rho_b c_b^2}\right)\left(\frac{\rho_b c_b}{\rho_a c_a}-\frac{\rho_a c_a}{\rho_b c_b}\right)\sin\left(\frac{\omega a}{c_a}\right)\sin\left(\frac{\omega b}{c_b}\right)$$
$$\left.+\frac{1}{2}\left(\frac{\rho_a c_a}{\rho_b c_b}+\frac{\rho_b c_b}{\rho_a c_a}\right)\left[\frac{\left(\frac{4}{3}\eta_a+\xi_a\right)a}{\rho_a c_a^3}\cos\left(\frac{\omega a}{c_a}\right)\sin\left(\frac{\omega b}{c_b}\right)+\frac{\left(\frac{4}{3}\eta_b+\xi_b\right)b}{\rho_b c_b^3}\sin\left(\frac{\omega a}{c_a}\right)\cos\left(\frac{\omega b}{c_b}\right)\right]\right\}. \quad (27)$$

Close to the edges of the Brillouin zone, where $k_x d \to \pm\pi$, the dissipation infinitively grows due to the factor $\sin(k_x d)$ in the denominator. Here, propagating wave becomes a standing wave and even very low viscosity leads to high dissipated power. Of course, the linear approximation fails in this region. Away from the band edges, the linear approximation is very close to the exact values of $k_x''$ calculated from Eq. (23). Frequency dependence of the attenuation coefficient for water-glycerol superlattice is given in Fig. 2. Material properties can be found in Table I. Near the edges of the bandgaps, the attenuation coefficient exhibits sharply non-monotonic behavior. Here, the difference between the exact and approximate values becomes essential.

At low frequencies, the graph $k_x''(\omega)$ in Fig. 2 is close to a parabola. The parabolic dependence is a signature of a homogeneous medium. In the low-frequency limit $\omega a/c_a,\ \omega b/c_b \ll 1$, a periodic structure homogenizes with effective elastic modulus $\lambda_{eff} = ((f/\lambda_a) + (1-f/\lambda_b))^{-1}$, effective mass density $\rho_{eff} = f\rho_a + (1-f)\rho_b$, and effective speed of sound $c_{eff} = \sqrt{\lambda_{eff}/\rho_{eff}}$. Here, $f = a/d$ is the filling fraction of material $a$. In the long-wavelength limit, Eq. (27) can be further simplified replacing sine functions by their arguments. After simple algebra, Eq. (27) yields $k_x'' \sim \omega^2$. Due to this quadratic scaling, the effective viscosity of a periodic structure

$$\frac{4}{3}\eta_{eff} + \xi_{eff} = \lambda_{eff}^2\left(f\frac{\frac{4}{3}\eta_a+\xi_a}{\lambda_a^2} + (1-f)\frac{\frac{4}{3}\eta_b+\xi_b}{\lambda_b^2}\right) \quad (28)$$

can be introduced through the attenuation coefficient [Eq. (9)] of the corresponding homogeneous effective medium, $k_x'' = (\omega^2/2\rho_{eff}c_{eff}^3)\left((4/3)\eta_{eff} + \xi_{eff}\right)$. Each layer of the viscous fluid gives an additive contribution to the effective viscosity with the weighting factors $\lambda_{eff}^2/\lambda_{a,b}^2$. Note that because of relatively low acoustic contrast between water and glycerol, the region of linear dispersion of sound extends practically to the first bandgap. The superlattice

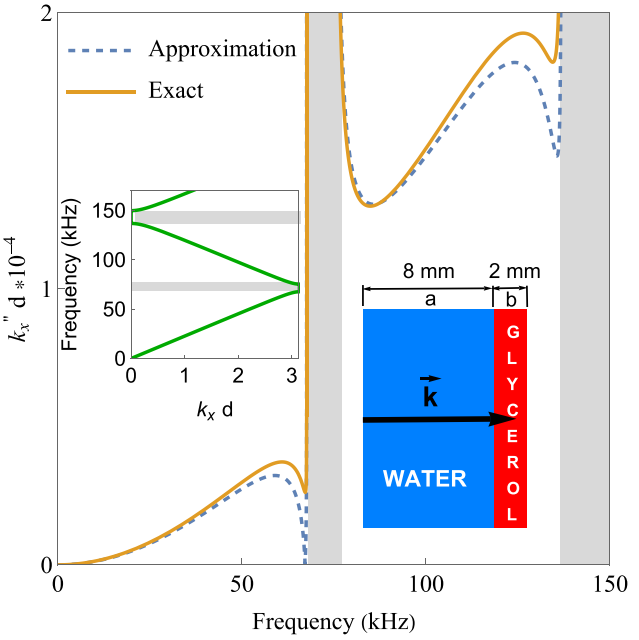


FIG. 2. (Color online) Frequency dependence of the attenuation coefficient of the longitudinal sound and normal incidence for water-glycerol superlattice with filling fraction of water $f = 0.8$. The exact result is calculated from Eq. (23) and the linear over viscosity approximation is given by Eq. (27). Both results exhibit fast growth near the band edge: the exact value remains finite and the approximate approaches infinity. Note that even for relatively high viscosity of glycerol, the decay length is on the order of $10^4$ lattice periods. The opposite case of very strong viscous absorption when the boundary layers overlap within the lattice period is numerically considered in Ref. 20. Left inset: the band structure of the water-glycerol superlattice. The bandgaps are shaded in gray. Right inset: the unit cell with geometrical parameters.

TABLE I. Density, elastic moduli, and viscosity of the materials used in the numerical calculations.

| Material | $\rho, \frac{\text{kg}}{\text{m}^3}$ | $\lambda$, GPa | $\eta$, Pa · s | $\mu$, GPa |
|---|---|---|---|---|
| Water | 1000 | 1.96 | 0.001 | — |
| Glycerol | 1200 | 3.072 | 0.9 | — |
| Polymethyl methacrylate (PMMA) | 1200 | 3 | — | 1.7 |

behaves as a homogeneous medium up to the frequency 50 kHz. The decay coefficient exhibits here the parabolic dependence on frequency and the effective viscosity can be evaluated from Eq. (28).

In the case of oblique incidence, the longitudinal and transverse modes are strongly coupled at the interface between two viscous fluids (or between viscous fluid and a solid). The exact dispersion equation obtained from the determinant Eq. (A1) becomes too cumbersome. It, however, can be essentially simplified assuming weak viscous losses. Due to formation of the viscous boundary layer $\delta$, the dissipated power scales as $\sqrt{\omega\eta}$. At frequencies $\omega \ll \omega^\star$, power dissipated in the bulk gives much less contribution since it scales as $\omega^2\eta$. While dissipation at oblique incidence exceeds greatly dissipation at normal incidence, we still assume that attenuation of sound remains weak, i.e., the wave propagates through the lattice without essential decay for many periods. The viscous boundary layer $\delta$ and the power dissipated within this layer originate from the last two equations of the set [Eq. (A1)] containing off diagonal elements $\sigma_{xy}$. The corresponding terms in the determinant [Eq. (A1)] lead (at oblique incidence) to the terms proportional to different powers of $\delta$ in the dispersion relation. Assuming weak dissipation, only the linear over $\delta \propto \sqrt{\eta}$ terms are left. The contribution of bulk dissipation proportional to different powers of $\eta$ and $\xi$ can usually be neglected except for a narrow interval of angles of propagation almost parallel to the superlattice axis. Within this narrow interval, a transition from dissipation in the boundary layer to dissipation in the bulk of the fluid occurs. This transition is analyzed in Sec. IV B, using the dispersion equation, where all the bulk dissipation terms are calculated exactly. Note that the terms of order $\delta^2 \propto \eta$ can be easily discriminated from the linear over $\eta$ bulk terms, since the $\delta^2$-contribution, being related to the boundary layer, vanishes at normal incidence. One more approximation that simplifies the dispersion relation is due to the limit $\tan((1+i)(a/\delta)) \to i$, valid if $\delta \ll a$. The latter condition is usually satisfied for a very wide range of frequencies. Taking into account the aforementioned approximations, the dispersion equation for the most practical case of fluid–solid superlattice is obtained in the following form:

$$
\begin{aligned}
&8\left[\alpha_1\alpha_2\sin(b\kappa_b)+\alpha_2k_y^2\sin(bk_b)+(1+i)\delta_a(\beta_0\cos(bk_b)+\beta_1\cos(b\kappa_b))\right]\cos(k_xd)\\
&\quad=-8\alpha_1k_y^2\sin(ak_a)-\left[\alpha_1-\alpha_2-k_y^2\right]^2\sin(x_1)-\left[\alpha_1+\alpha_2-k_y^2\right]^2\sin(x_2)+\left[\alpha_1-\alpha_2+k_y^2\right]^2\sin(x_3)\\
&\qquad+\left[\alpha_1+\alpha_2+k_y^2\right]^2\sin(x_4)+(1+i)\delta_a\Big[-(\alpha_1-\alpha_2-k_y^2)(\beta_2-\beta_3+\beta_4)\cos(x_1)\\
&\qquad+(\alpha_1+\alpha_2-k_y^2)(\beta_2+\beta_3-\beta_4)\cos(x_2)-(\alpha_1-\alpha_2+k_y^2)(\beta_2-\beta_3-\beta_4)\cos(x_3)\\
&\qquad+(\alpha_1+\alpha_2+k_y^2)(\beta_2+\beta_3+\beta_4)\cos(x_4)+\beta_5\cos(ak_a)\Big].
\end{aligned}
\tag{29}
$$

Here,

$$
\begin{aligned}
&\alpha_1=\frac{(\omega^2-2c_t^2k_y^2)^2c_b}{4c_t^3\sqrt{(\omega^2-c_b^2k_y^2)(\omega^2-c_t^2k_y^2)}},\quad \alpha_2=\frac{\rho_a\omega^4c_a}{4\rho_bc_t^3\sqrt{(\omega^2-c_a^2k_y^2)(\omega^2-c_t^2k_y^2)}},\\
&\beta_0=\frac{k_y^2\rho_a\omega^4(\omega^2(\rho_a/\rho_b-1)+2c_t^2k_y^2)c_ac_b}{8\rho_bc_t^5\sqrt{(\omega^2-c_a^2k_y^2)(\omega^2-c_b^2k_y^2)(\omega^2-c_t^2k_y^2)}},\quad \beta_1=\frac{\rho_a\omega^4(\omega^2\rho_a/\rho_b+2c_t^2k_y^2)(\omega^2-2c_t^2k_y^2)c_ac_b}{16\rho_bc_t^7\sqrt{(\omega^2-c_a^2k_y^2)(\omega^2-c_b^2k_y^2)(\omega^2-c_t^2k_y^2)}},\\
&\beta_2=\frac{\rho_a\omega^4c_b}{4\rho_bc_t^4\sqrt{\omega^2-c_b^2k_y^2}},\quad \beta_3=\frac{(\omega^2\rho_a/\rho_b+2c_t^2k_y^2)^2c_a}{4c_t^4\sqrt{\omega^2-c_a^2k_y^2}},\quad \beta_4=\frac{k_y^2(\omega^2(\rho_a/\rho_b-1)+2c_t^2k_y^2)^2c_ac_b}{4c_t^3\sqrt{(\omega^2-c_a^2k_y^2)(\omega^2-c_b^2k_y^2)(\omega^2-c_t^2k_y^2)}},\\
&\beta_5=\frac{k_y^2(\omega^2-2c_t^2k_y^2)(\omega^2\rho_a/\rho_b+2c_t^2k_y^2)(\omega^2(\rho_a/\rho_b-1)+2c_t^2k_y^2)c_ac_b}{c_t^5\sqrt{(\omega^2-c_a^2k_y^2)(\omega^2-c_b^2k_y^2)(\omega^2-c_t^2k_y^2)}}.
\end{aligned}
\tag{30}
$$

The subindex $a(b)$ is related to viscous fluid (elastic solid). The direction of propagation is fixed by the transverse wave vector component $k_y$, which is given by the angle of incidence of the external excitation and it is conserved during wave refraction at the superlattice interfaces. Together with frequency $\omega$, these two parameters completely define the Bloch wave in the layered structure. The longitudinal components of the wave vectors in the fluid and solid layers are obtained from the local dispersion relations

https://doi.org/10.1121/10.0024719

$$k_a^2+k_y^2=\frac{\omega^2/c_a^2}{1-i\dfrac{\omega}{\rho_a c_a^2}\left(\dfrac{4}{3}\eta_a+\xi_a\right)},\quad c_a^2=\frac{\lambda_a}{\rho_a},$$
$$k_b^2+k_y^2=\frac{\omega^2}{c_b^2},\quad c_b^2=\frac{\lambda_b+2\mu_b}{\rho_b},$$
$$\kappa_b^2+k_y^2=\frac{\omega^2}{c_t^2},\quad c_t^2=\frac{\mu_b}{\rho_b}. \tag{31}$$

Other notations in Eq. (29) are defined as

$$x_1=ak_a-b(k_b-\kappa_b),\quad x_2=ak_a+b(k_b-\kappa_b),$$
$$x_3=ak_a-b(k_b+\kappa_b),\quad x_4=ak_a+b(k_b+\kappa_b). \tag{32}$$

The limiting case when $\delta_a,\eta_a,\xi_a=0$ corresponds to completely the disssipationless structure of elastic solid and ideal fluid. In this case, the dispersion equation becomes real

$$\begin{aligned}8\left[\alpha_1\alpha_2\sin(b\kappa_b)+\alpha_2 k_y^2\sin(bk_b)\right]\cos(k_x d)&\\ =-8\alpha_1 k_y^2\sin(ak_a)-\left[\alpha_1-\alpha_2-k_y^2\right]^2\sin(x_1)&\\ -\left[\alpha_1+\alpha_2-k_y^2\right]^2\sin(x_2)+\left[\alpha_1-\alpha_2+k_y^2\right]^2&\\ \times\sin(x_3)+\left[\alpha_1+\alpha_2+k_y^2\right]^2\sin(x_4).&\end{aligned} \tag{33}$$

Equation (33) coincides with the result reported in Ref. 34.

In the special case of a normal incidence of longitudinal sound wave, the boundary layer is not formed and dissipation occurs in the bulk of viscous fluid. The dispersion relation accounting for the dissipative losses in the bulk and oblique propagation can be written in the same form as Eq. (29) but the parameters $\alpha$ and $\beta$ are redefined. General formulas for these parameters are given in Appendix B [see Eq. (B1)]. Note that the local dispersion relations [Eq. (31)] include bulk dissipation. In the case of normal incidence, the dispersion relation [Eq. (29)] with parameters given by Eq. (B1) is simplified to the following form:

$$\begin{aligned}\cos(k_x d)=\cos(ak_a)\cos(bk_b)&\\ +\frac{1}{2}\left(\frac{k_a\left(\lambda_a-\frac{4}{3}i\omega\eta_a-i\omega\xi_a\right)}{k_b(\lambda_b+2\mu_b)}\right.&\\ \left.+\frac{k_b(\lambda_b+2\mu_b)}{k_a\left(\lambda_a-\frac{4}{3}i\omega\eta_a-i\omega\xi_a\right)}\right)&\\ \times\sin(ak_a)\sin(bk_b).&\end{aligned} \tag{34}$$

Equation (34) coincides with Eq. (23), providing that the local dispersion relations [Eq. (31)]are satisfied.

## IV. ANALYSIS OF ATTENUATION OF SOUND IN SUPERLATTICES WITH DIFFERENT CONSTITUENTS

### A. Unit cell of viscous and ideal fluids

In a superlattice where the layer $a$ is a viscous fluid and the layer $b$ is an ideal fluid ($\eta_b=0$), the dispersion relation [Eq. (29)] can be simplified to the following form:

$$\begin{aligned}\cos(k_x d)=\cos(ak_a)\cos(bk_b)&\\ -\frac{1}{2}\left[\frac{\omega\rho_b k_a}{(\omega\rho_a+2i\eta_a k_y^2)k_b}+\frac{(\omega\rho_a+2i\eta_a k_y^2)k_b}{\omega\rho_b k_a}\right]&\\ \times\sin(ak_a)\sin(bk_b)&\\ -2ik_y^2\eta_a\delta_a\left[\frac{k_a}{\omega\rho_a+2i\eta_a k_y^2}\sin(ak_a)\cos(bk_b)\right.&\\ \left.+\frac{k_b}{\omega\rho_b}\sin(bk_b)\cos(ak_a)\right].&\end{aligned} \tag{35}$$

In the quasistatic limit $\omega,k_x\to 0$, the complex Bloch vector $k_x=k_x'+ik_x''$ can be calculated explicitly

$$\frac{k_x^2d^2}{2}\approx\left(\frac{k_x'^2}{2}+ik_x'\ k_x''\right)d^2=\omega^2\frac{(a\rho_a+b\rho_b)}{2\lambda_a\lambda_b}\left[a\lambda_b+b\lambda_a-(b\lambda_a c_b^2+a\lambda_b c_a^2)\frac{\sin^2(\theta_a)}{c_a^2}\right]$$
$$+i\frac{2\sqrt{2}\eta_a^{3/2}\omega^{5/2}[a\lambda_b+b\lambda_a-(b\lambda_a c_b^2+a\lambda_b c_a^2)(\sin(\theta_a)/c_a)^2]}{\sqrt{\rho_a}\lambda_a\lambda_b}\left(\frac{\sin(\theta_a)}{c_a}\right)^2. \tag{36}$$

The imaginary part of the right-hand side of Eq. (36) is proportional to $\sin^2(\theta_a)$, i.e., it contributes to dissipation only at oblique incidence. The decay coefficient scales as $k_x''\propto(\omega\eta)^{3/2}$, which is different from the scaling of dissipation at solid–viscous or viscous–viscous interface. This qualitative difference is due to lack of shear modulus in an ideal fluid. At normal incidence, dissipation is due solely to the losses in the bulk of viscous fluid. These losses are omitted in Eq. (36).

In a special case, when the viscous layer is sufficiently thin, the dissipative losses vanish at the frequency of Bragg

reflection. In x-ray diffraction, the effect of anomalous transmission through a crystal was observed by Borrmann in 1941.[35] Optical analog of the Borrmann effect in 1D photonic crystals with absorbing layers was observed in Refs. 36 and 37. Anomalous transmission of sound through a periodic set of absorbing porous sheets in air was reported in Ref. 38. The peaks of transmission are close to the positions of the bandgaps, where transmission is usually suppressed. Theoretical treatment of this acoustic analog of the Borrmann effect was reported in Ref. 39 where porous sheets are considered as $\delta$-like resistive scatterers. Acoustic resistance of a narrow porous layer gives rise to a jump discontinuity of acoustic pressure at each sheet.

Borrmann effect in acoustics may be realized in a superlattice of narrow layers of high-viscosity fluid and thick layers of ideal fluid. Let the thickness $a$ of the viscous layer be much less than the wavelength. At the same time, the thickness $a$ exceeds much the thickness of the boundary layer, viz.,

$$\delta_a\omega/c_a \ll a\omega/c_a \ll 1. \tag{37}$$

Expanding trigonometric functions in Eq. (35) and keeping liner over $a\eta_a$ terms, the following dispersion equation is obtained:

$$\cos(k_x d) = \cos(k_b d) - iU\sin(k_b d),$$
$$k_{a,b} = \sqrt{\left(\frac{\omega}{c_{a,b}}\right)^2 - k_y^2}, \tag{38}$$

where

$$U = (ak_a'')\frac{\omega\rho_b}{k_b c_a \rho_a} + \frac{a\delta_a^2 k_y^2}{2k_b}\left(k_b^2\frac{\rho_a}{\rho_b} - k_a^2\frac{\rho_b}{\rho_a}\right). \tag{39}$$

It is clear that dissipation vanishes at the frequencies of Bragg's diffraction where $\sin(k_b d) = 0$. Figure 3 shows the angular dependance of the decay coefficient for two frequencies of 35 and 60 kHz. Very narrow deep minima appear exactly at the Bragg's frequencies. The same dispersion equation was obtained for the superlattice with resistive scatterers.[39] The strength of the parameter $U$ is proportional to the amplitude of jump discontinuity of pressure. Here, the nature of the parameter $U$ is related to viscosity of the layer $a$. The first term in Eq. (39) is due to dissipation in the bulk. It is proportional to the decay coefficient of the longitudinal mode [Eq. (9)] in free fluid, $k_a'' = \omega^2\left(\frac{4}{3}\eta_a + \xi_a\right)/(2\rho_a c_a^3)$. While the second term contains the thickness $\delta_a^2$ and it vanishes at normal incidence, $k_y = 0$, it cannot be associated with dissipation in the boundary layer since the layer is not formed at the interface with ideal fluid. Also, dissipation in the boundary layer is proportional to $\delta_a$. This term, as well as the first term, is the contribution of the bulk dissipation modified by multiple scattering at oblique incidence.

Assuming that the speeds of sound in the viscous and ideal fluid do not differ much, it is easy to see that both terms contributing to $U$ are small parameters. The first term

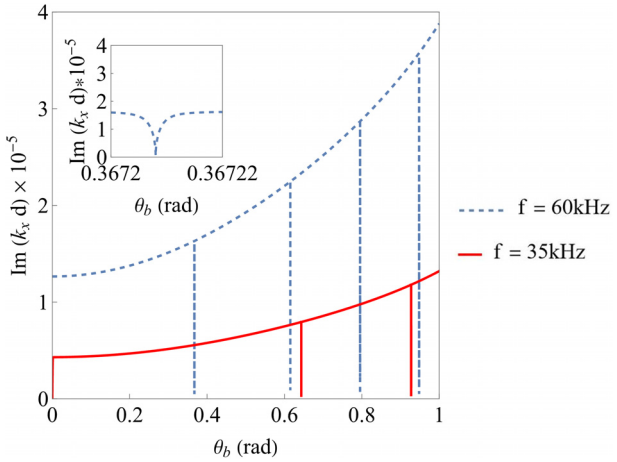


FIG. 3. (Color online) Borrmann effect. Angular dependence of the dimensionless decay coefficient for a superlattice with narrow ($a = 1$ mm) viscous layer of glycerol and thick layer ($b \approx d = 100$ mm) of inviscid water. Inset shows the fine structure of deep minima near the frequencies of Bragg scattering.

$\sim ak_l'' \ll 1$ since the decay length of sound $1/k_l''$ is much longer than the period of the lattice. The second term $\sim a\delta_a^2/\lambda^3 \ll 1$ since $a$ and $\delta_a$ are small in comparison with the wavelength $\lambda$. If the angle of incidence is not small, i.e., $k_y \sim k_x$, both terms are of the same order of magnitude. This can be seen by expressing each term through density, viscosity, and frequency. Thus, the Borrmann effect may be observed in transmission of sound through a superlattice with narrow viscous layers. The structure of the resonant peaks in the transmission coefficient was analyzed in details in Ref. 39.

### B. Unit cell of two different viscous fluids

If both layers in the unit cell are different viscous fluids, for example, water and glycerol, the dispersion equation becomes more complicated due to existence of two boundary layers, $\delta_a$ and $\delta_b$. The dispersion equation is obtained from the determinant Eq. (A1) assuming weak dissipation. Keeping the linear over $\delta_a$ and $\delta_b$ terms and all the terms related to bulk dissipation, the dispersion equation can be reduced to the following form:

$$\begin{aligned}\cos(k_x d) = {}& \cos(ak_a)\cos(bk_b) \\ & - \frac{1}{2}\left[\frac{k_b(\rho_a\omega + 2i\eta_a k_y^2)}{k_a(\rho_b\omega + 2i\eta_b k_y^2)} + \frac{k_a(\rho_b\omega + 2i\eta_b k_y^2)}{k_b(\rho_a\omega + 2i\eta_a k_y^2)}\right] \\ & \times \sin(ak_a)\sin(bk_b) \\ & - \frac{ik_y^2\delta_a\delta_b(\rho_a - \rho_b)[(\rho_a - \rho_b)\omega + 2i(\eta_a - \eta_b)k_y^2]}{2(\delta_a\rho_a + \delta_b\rho_b)} \\ & \times \left[\frac{\cos(ak_a)\sin(bk_b)}{k_b(\rho_a\omega + 2i\eta_a k_y^2)} + \frac{\sin(ak_a)\cos(bk_b)}{k_a(\rho_b\omega + 2i\eta_b k_y^2)}\right].\end{aligned} \tag{40}$$

This dispersion relation is symmetric over indices $a$ and $b$. Note that while the last term contains quadratic over $\delta_a$ and

https://doi.org/10.1121/10.0024719

$\delta_b$ contribution in the numerator, it is kept due to the presence of a linear combination of deltas in the denominator. In the quasistatic limit, the decay coefficient can be explicitly obtained from Eq. (40):

$$\begin{aligned}\frac{k_x^2 d^2}{2} &\approx \left(\frac{k_x'^2}{2} + ik_x' k_x''\right) d^2 \\ &= \omega^2 \frac{(a\rho_a + b\rho_b)}{2\lambda_a\lambda_b}\left[a\lambda_b + b\lambda_a - (b\lambda_a c_b^2 + a\lambda_b c_a^2)\frac{\sin^2(\theta_a)}{c_a^2}\right] \\ &+ \frac{i\omega^{3/2}(\rho_a-\rho_b)^2(a\rho_a+b\rho_b)\sqrt{\eta_a\eta_b}}{\sqrt{2}(\rho_a\rho_b)^{3/2}\left(\sqrt{\eta_a\rho_a}+\sqrt{\eta_b\rho_b}\right)}\left(\frac{\sin(\theta_a)}{c_a}\right)^2 \\ &+ i\omega^3\frac{a\rho_a+b\rho_b}{2}\left[\frac{a\left(\frac{4}{3}\eta_a+\xi_a\right)}{\lambda_a^2}+\frac{b\left(\frac{4}{3}\eta_b+\xi_b\right)}{\lambda_b^2}\right] \\ &+ i\omega^3 ab\left[\left(\frac{\eta_b}{\lambda_a}+\frac{\eta_a}{\lambda_b}-\frac{\eta_b\rho_a}{\lambda_b\rho_b}-\frac{\eta_a\rho_b}{\lambda_a\rho_a}\right)\left(\frac{\sin(\theta_a)}{c_a}\right)^2\right. \\ &\left.+\left[\frac{\eta_b\rho_a}{\rho_b^2}+\frac{\eta_a\rho_b}{\rho_a^2}-\frac{\eta_a}{\rho_b}-\frac{\eta_b}{\rho_a}\right]\left(\frac{\sin(\theta_a)}{c_a}\right)^4\right]. \qquad (41)\end{aligned}$$

The real parts of Eqs. (36) and (41) are the same since both of them give linear dispersion relation $\omega = c_{eff}k$ in the corresponding homogenized medium with $c_{eff} = \sqrt{\lambda_{eff}/\rho_{eff}}$. The symmetry over indices $a$ and $b$ remains true since $\sin\theta_a/c_a = \sin\theta_b/c_b$.

The imaginary part of the Bloch vector $k_x''$ calculated from Eq. (41) contains contributions of order $\sqrt{\omega}$ and $\omega^2$, which are due to dissipation in the boundary layers and in the bulk of the fluids, respectively. The boundary-layer contribution vanishes for small angles of incidence when $\theta_a \to 0$. It also vanishes if $\rho_a \to \rho_b$. This effect is a manifestation of the Third Newton's Law when two surfaces interacting only through friction forces are equally accelerated if their densities are the same. Due to equal acceleration, viscous friction between two very viscous fluids with close densities is strongly suppressed. If the angle $\theta_a$ is not small, the sound decay is due to dissipation in the boundary layers and $k_x'' \propto \sqrt{\omega}$. This term scales with viscosities as $(\sqrt{\omega}\sqrt{\eta_a\eta_b})/(\sqrt{\eta_a\rho_a}+\sqrt{\eta_b\rho_b})$, which is a generalization of $\sqrt{\omega\eta}$ scaling for solid–fluid interface.

The boundary-layer term $\propto \omega^{3/2}\sin^2\theta_a$ in Eq. (41) contributes to dissipation only at oblique incidence. A smooth transition from dissipation in the boundary layer to dissipation in the bulk occurs within a narrow interval of angles near $\theta_a = \Theta$. Frequency dependence of the attenuation coefficient $k_x''$ changes from $\omega^2$ at $\theta_a < \Theta$ to $\sqrt{\omega}$ at $\theta_a > \Theta$. This transition is shown in Fig. 4. It is clear that the decay coefficient grows fast with angle $\theta_a$ due to change of the dissipation mechanism from the bulk one to dissipation in the boundary layer. Equation (41) was used to plot Fig. 4. From the same equation, the estimate for the transition angle

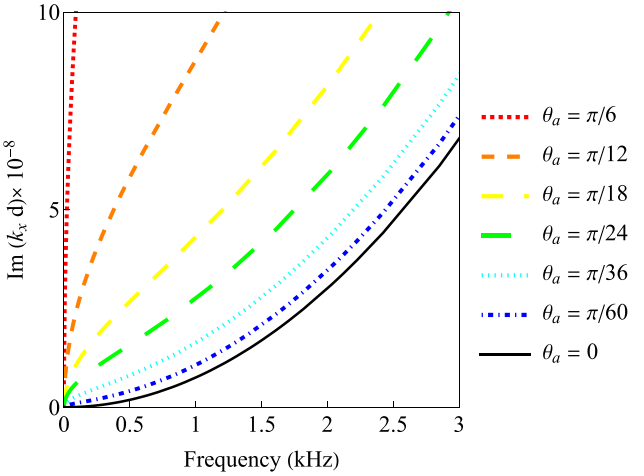


FIG. 4. (Color online) Graphs showing the transition from $\omega^2$ (dissipation in the bulk) to $\sqrt{\omega}$ (dissipation in the boundary layer) dependence for the decay coefficient with increasing angle of incidence $\theta_a$ in the quasistatic region where the Bloch vector is obtained from Eq. (41). At a given frequency, the transition occurs within a narrow interval of angles near the angle $\Theta$ defined by Eq. (42).

$\theta_a = \Theta$ can be obtained by equating the imaginary term $\propto \omega^{3/2}\sin^2\theta_a$, which is responsible for attenuation in the boundary layer, to the $\theta_a$-independent imaginary term $\propto \omega^3$ contributing to the bulk attenuation

$$\left(\frac{\sin(\Theta)}{c_a}\right)^2 = \frac{\omega^{3/2}}{\sqrt{2}}\frac{(\rho_a\rho_b)^{3/2}}{(\rho_a-\rho_b)^2}\left(\sqrt{\frac{\rho_a}{\eta_b}}+\sqrt{\frac{\rho_b}{\eta_a}}\right) \times\left(a\frac{\frac{4}{3}\eta_a+\xi_a}{\lambda_a^2}+b\frac{\frac{4}{3}\eta_b+\xi_b}{\lambda_b^2}\right). \qquad (42)$$

The angle $\Theta$ increases with frequency ($\Theta \propto \omega^{3/4}$) that can be seen in Fig. 4 where the transition from the concave to convex part is shifted to higher frequencies with $\theta_a$. Dependance on viscosity is nonmonotonic due to the presence of two competing terms in the numerator and denominator. If the viscosity $\eta_a$ is fixed, the transition angle grows $\sim\eta_b^{-1/4}$ for $\eta_b \to 0$. In the region $\eta_b > \eta_a$, it increases as $\eta_b^{1/2}$. Of course, these asymptotics are valid as long as $\Theta < 1$. The graphs in Fig. 5 show the dependance $\Theta(\eta_b)$ for different values of $\eta_a$ at frequency 2 kHz, which lies in the region of linear dispersion.

At normal incidence, the effective viscosities [Eq. (28)] can be introduced. They do not depend on frequency and linearly depend on the filling fraction $f$. At oblique incidence, the effective viscosity $\eta$ becomes frequency dependent; therefore, it is more convenient to work with the decay coefficient $k_x''$, for which dependence on the filling fraction is obtained from Eq. (41). This dependence is shown in Fig. 6 for frequency 20 kHz which lies well below the first bandgap. Since the thickness of each layer must be much longer than the boundary layer thickness, $\delta_a, \delta_b \ll a, (d-a)$, the filling fraction of glycerol in Fig. 6 lies within $0.1 < f < 0.9$. The decay coefficient increases fast with the thickness of the more viscous fluid (glycerol). Similar

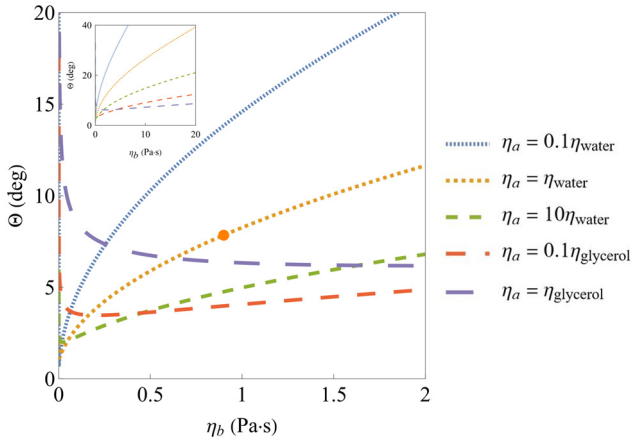


FIG. 5. (Color online) Nonmonotonic dependence $\Theta(\eta_b)$ for different $\eta_a$ at frequency 2 kHz. All the mechanical parameters, except shear viscosity, correspond to water ($a = 8$ mm) and glycerol ($b = 2$ mm). In a superlattice of real water and glycerol, the transition from dissipation in the bulk to dissipation in the boundary layer occurs at relatively small angle $\Theta = 7.8°$ shown by the orange dot. Inset shows the same dependence for a wider range of viscosity $\eta_b$.

behavior was predicted for 2D phononic crystal[23,24] where the circumference of the solid rods (and then, the length of the boundary layer) increases with the filling fraction as $\sqrt{f}$. For 1D phononic crystal, the area covered by both boundary layers does not change with the filling fraction. The dependence $k_x''(f)$ appears because for larger filling fractions, the less viscous fluid (water) is gradually replaced by glycerol with viscosity almost $10^3$ of the viscosity of water. Thus, the physical reason for strong $f$-dependence in Fig. 6 is not related to the dissipation in the boundary layers. It is due to high viscosity contrast and to the contribution of bulk dissipation in glycerol, which cannot be neglected.

### C. Unit cell of viscous fluid and dissipationless solid

Solid–fluid layered structure is feasible for experimental realization. We assume that sound wave decays much

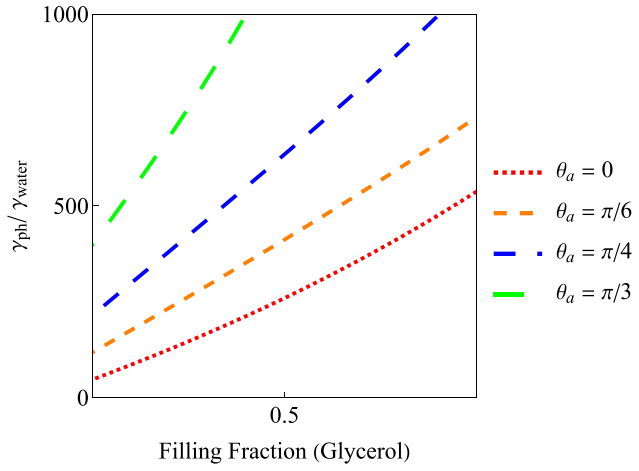


FIG. 6. (Color online) Decay coefficient for water-glycerol superlattice $\gamma_{ph} = k_x''(f)$ normalized to the decay coefficient of water ($\gamma_{water}$) vs filling fraction $f$ of glycerol. Strong dependence on the filling fraction is related to the high viscosity contrast between water and glycerol, $\gamma_{glyc}/\gamma_{water} = 1.6 \times 10^3$.

less in the solid layer; therefore, its elastic coefficients $\lambda_b$ and $\mu_b$ are real. Although the dispersion equation for solid–fluid superlattice [Eq. (29)] looks more complicated than that for fluid–fluid structure [Eq. (40)], the frequency and angular dependencies of the decay coefficient $k_x''$ remain qualitatively the same. For normal incidence, only the bulk mechanism of dissipation with the decay coefficient $\propto \eta_a\omega^2$ contributes to the decay of sound wave. In the case of an oblique incidence, viscous dissipation prevails and scales as $\sqrt{\eta_a\omega}$.

Behavior of the decay coefficient within a wideband of frequencies for water-poly(methyl methacrylate (PMMA) structure is plotted in Fig. 7. At very low frequencies where superlattice homogenizes, the decay coefficient exhibits $\sqrt{\omega}$ dependence due to Konstantinov's effect at oblique incidence. At higher frequencies, the dispersion of sound becomes nonlinear and frequency dependence of the Bloch vector is obtained from the quite complicated Eq. (29). Near the band edges, the Bloch wave becomes a standing wave that leads to very fast growth of viscous losses. At the band edge, the viscous losses are an order of magnitude higher than within the transmission zone. However, the Bloch wave remains a propagating mode since still $k_x''d \ll 1$. Only within the bandgap the wave essentially decays at a distance of the lattice period, but this decay is due to Bragg scattering. Viscous losses remain relatively low because of low viscosity of water. For a finite-length lattice, even low viscosity losses play an important role within the bandgap

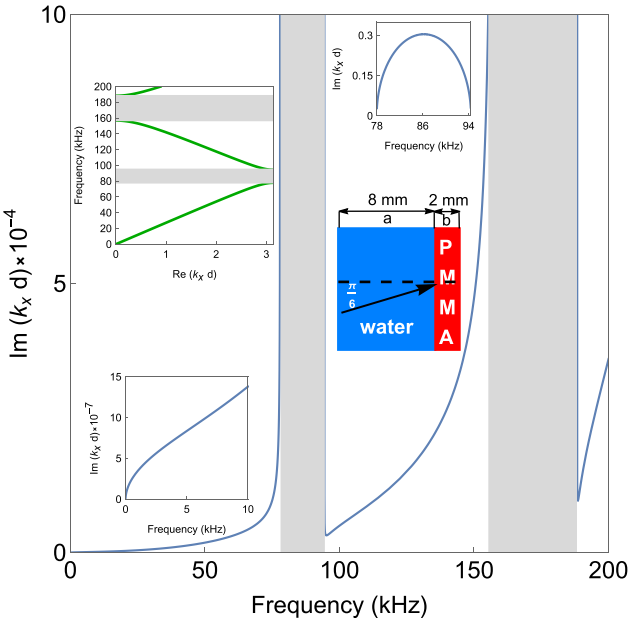


FIG. 7. (Color online) Frequency dependence of the dimensionless decay coefficient for water-PMMA superlattice calculated from Eq. (29) for the filling fraction $f = 0.2$. The region within the two lowest transmission bands is shown. Shaded regions are the bandgaps of the band structure shown in the left top inset. Left bottom inset is the decay coefficient at very low frequencies where $k_x'' \propto \sqrt{\omega}$. Right top inset is the decay coefficient within the first bandgap. Left bottom inset shows the direction of propagation within the unit cell. Note order-of-magnitude difference in the decay coefficient at low frequencies, close to the band edge, and within the bandgap.

https://doi.org/10.1121/10.0024719

frequencies increasing the tunneling time of a pulse through the sample.[40]

The dependence of the decay coefficient $\gamma_{ph} = k_x''$ on the filling fraction of solid PMMA is obtained from Eq. (29). This dependence is plotted in Fig. 8 for different angles of incidence and frequency 20 kHz. This frequency is well below the bandgap as shown in Fig. 7. For normal incidence (blue curve), the dissipation is very low. The right inset shows how the decay coefficient decreases from its value in water ($f = 0.1$) to practically zero value in a superlattice with very small content of water ($f = 0.9$). For very small angles of incidence, $\theta_a < 0.03$, when attenuation is due to dissipation in the bulk, the decay coefficient still decreases with the filling fraction of solid. This can be seen in the left inset to Fig. 8. Also, for larger angles, $\theta_a > 0.03$, this tendency is changed to the opposite one due to the increasing contribution of the dissipation within the boundary layer $\delta$. Once the boundary-layer contribution becomes dominant, the decay coefficient becomes larger by orders of magnitude. Dissipation occurs within the boundary layer $\delta$ and the rest amount of viscous fluid does not contribute to attenuation of sound. While $\delta$ does not change with $f$ (for $a \gg \delta$), the decay coefficient in Fig. 8 smoothly grows with decreasing of the fraction of the viscous constituent, as it is seen in Fig. 8. Such "abnormal" dependence is due to variation of the effective mechanical parameters, $c_{eff}$ and $\rho_{eff}$, with the filling fraction.

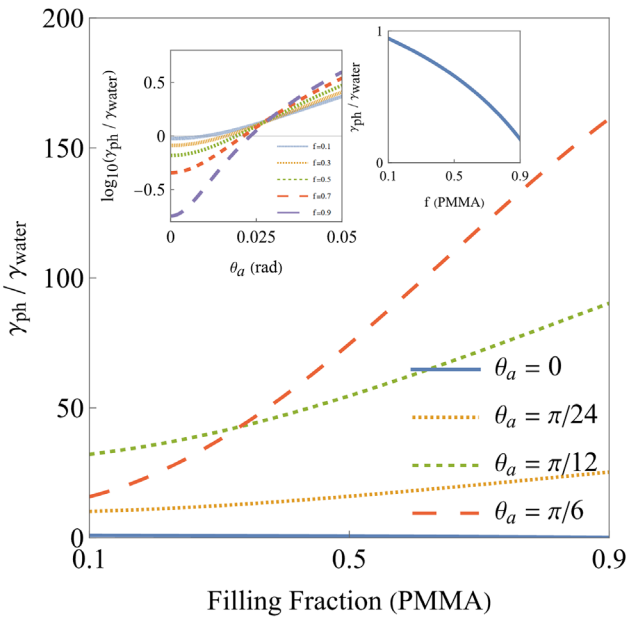


FIG. 8. (Color online) Normalized decay coefficient vs filling fraction for water-PMMA superlattice for different angles of incidence. The frequency of sound is 20 kHz. The right inset shows the case of normal incidence when dissipation occurs in the whole bulk of water. The left inset shows how dissipation in the bulk changes to dissipation within the boundary layer with increasing angle of incidence for different filling fractions. For angles $\theta_a > 0.03$, the decay coefficient exhibits "abnormal" increasing dependence with decreasing amount of viscous water. The curves appear to cross at the same point but on the enlarged picture, there are several crossing points within a narrow region near $\theta_a = 0.03$.

The angular dependence of the decay coefficient at fixed filling fraction exhibits a strong anomaly related to a specific nature of wave conversion at a boundary between solid and fluid. Due to the presence of transverse and longitudinal modes in the solid layer and only a single longitudinal mode in the fluid layer, so-called transmission zeros appear in the spectrum of a solid plate immersed in ideal fluid if the angle of incidence does not exceed the critical value[32,33]

$$\theta_c = \arcsin \frac{V_f/V_t}{2\sqrt{1 - V_t^2/V_l^2}}, \tag{43}$$

where $V_f$, and $V_t$, $V_l$ are the phase velocities of sound in fluid and solid, respectively. For water-PMMA boundary, the critical angle is 0.756 rad. In a series of curves in Fig. 9, giving the angular dependence of the decay coefficient for different viscosities anomalously high decay appears close to $\theta_c = 0.756$. The position of the peak depends slightly on the viscosity of fluid due to the imaginary terms in the dispersion relation. A dissipationless solid–fluid bilayer structure becomes nontransparent when the factor for $\cos(k_x\ d)$ in the left-hand-side of Eq. (33) vanishes,[32,33]

$$\alpha_1\alpha_2 \sin(b\kappa_b) + \alpha_2 k_y^2 \sin(bk_b) = 0. \tag{44}$$

Therefore, in Fig. 9, the decay coefficient tends to infinity at $\theta_c = 0.756$ for inviscid fluid. Note that in the low-frequency limit, the solution of Eq. (44) gives the result for the critical angle [Eq. (43)]. In the case of a viscous fluid, the corresponding term in Eq. (29) acquires imaginary part. This term remains very small but finite at the critical angle, giving rise to a large but finite attenuation coefficient in Fig. 9. Dissipation for $\theta_a > \theta_c$ exceeds that by 2–3 orders of magnitude at smaller angles of incidence. Here, the level of dissipation does not change much with the angle but it strongly depends on viscosity. It is obvious that the sound absorption at $\theta_a > \theta_c$ is pure dissipative but the reason for anomalously high decay remains unclear. This requires more detailed study.

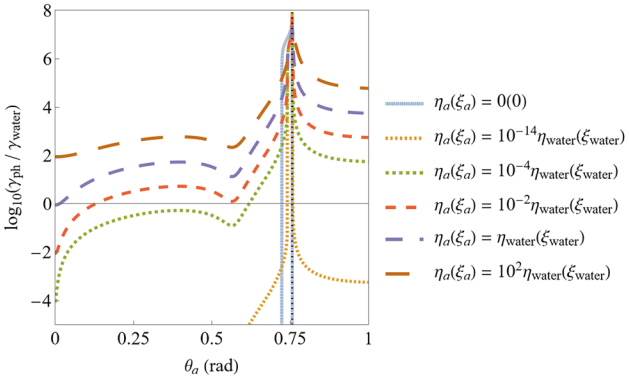


FIG. 9. (Color online) Angular dependence of the normalized decay coefficient of water-PMMA superlattice at filling fraction $f = 0.2$ and frequency 20 kHz. Note the logarithmic scale on the vertical axis. Dashed line shows the position of the critical angle for inviscid fluid [Eq. (43)].

## V. CONCLUSIONS

We derived and analyzed the dispersion equation for sound waves propagating in a periodic layered heterogeneous structure containing at least one viscous fluid as a constituent. The derivation of the dispersion equation is based on the Navier–Stokes equation for sound wave and the boundary conditions of continuity of fluid displacement and stresses at the interfaces plus Bloch periodic boundary condition. The boundary conditions result in vanishing $8 \times 8$ determinant. The obtained dispersion equation is very general; it is valid for different combinations of elastic layers, any direction of propagation, and frequency of sound. It was analyzed for normal and oblique incidence. In the region of low frequencies where a superlattice behaves as a homogeneous medium with effective speed of sound, the decay coefficient of sound wave is proportional to $\omega^2\eta$ at normal incidence, where $\eta$ plays a role of corresponding effective viscosity. This behavior is a signature of viscous dissipation in the bulk of the fluid. For oblique incidence, the decay coefficient scales as $\sqrt{\omega\eta}$ that corresponds to much stronger decay within a narrow boundary layer. The transition from dissipation in the bulk to dissipation in the boundary layer occurs within a narrow range of frequencies. At frequencies close to a band edge, dissipation strongly increases because a propagating Bloch wave becomes a standing wave. In a special case of viscous and ideal fluid constituents, the boundary layer is not formed, leading to unusual scaling of the decay coefficient, $k_x'' \propto (\omega\eta)^{3/2}$. In the case of superlattice consisting of narrow layers with high viscosity fluid and layers of ideal fluid, an acoustic analog of the Borrmann effect is predicted. Unlike previous studies of the acoustic Borrmann effect,[38,39] our result for anomalous transmission does not require the presence of jump discontinuity of pressure at narrow layers. It can be observed in a periodic structure of layers with high contrast of viscosities.

The reported results serve as a supplement to the theory of phononic crystals with viscoelastic constituents. Since in the case of 1D periodicity the dispersion equation is known in an explicit form, many results obtained in the limit of weak viscosity can be presented analytically and within a wide range of parameters,[3,4,7,19] unlike the cases of 2D and 3D periodicity,[8,41–43] where analytical results for the decay length are available only in the long-wavelength limit.[22–24] Analytical results are more valuable since, in many cases, the numerical methods of calculation of transmission through a long, multilayered system with low-viscosity constituents (air or water), turn out to be unsuccessful. Finite-difference methods require high machine precision incompatible with memory capabilities of standard computers. The reported results are quite universal, being available for design of acoustic devices, which require low or high absorption. In particular, multi-wall and multilayered structures are widely used in road construction[1] and in architecture for soundproofing.[44,45]

## ACKNOWLEDGMENTS

This work is supported by an EFRI Grant No. 1741677 from the National Science Foundation and by the Air Force Office of Scientific Research under award No. FA9550-23-1–0630.

## AUTHOR DECLARATIONS

### Conflict of Interest

The authors have no conflicts to disclose.

## DATA AVAILABILITY

The data that support the findings of this study are available from the corresponding author upon reasonable request.

## APPENDIX A: DERIVATION OF THE DISPERSION RELATION

Substituting the velocities [Eqs. (14) and (15)] with Eq. (13) and calculating the components $\sigma_{xx}$ and $\sigma_{xy}$ of the stress tensor [Eq. (21)] for each layer, all the necessary elements of the set of homogeneous equations [Eq. (20)] are obtained. The nontrivial solutions of this set exist if the following determinant vanishes:

$$\det\begin{pmatrix}
-e^{iak_a}k_a & e^{-iak_a}k_a & e^{ia\kappa_a}k_y & e^{-ia\kappa_a}k_y & e^{iak_b}k_b & -e^{-iak_b}k_b & -e^{ia\kappa_b}k_y & -e^{-ia\kappa_b}k_y \\
-e^{idk_x}k_a & e^{idk_x}k_a & e^{idk_x}k_y & e^{idk_x}k_y & e^{idk_b}k_b & -e^{-idk_b}k_b & -e^{id\kappa_b}k_y & -e^{-id\kappa_b}k_y \\
-e^{iak_a}k_y & -e^{-iak_a}k_y & -e^{ia\kappa_a}\kappa_a & e^{-ia\kappa_a}\kappa_a & e^{iak_b}k_y & e^{-iak_b}k_y & e^{ia\kappa_b}\kappa_b & -e^{-ia\kappa_b}\kappa_b \\
-e^{idk_x}k_y & -e^{idk_x}k_y & -e^{idk_x}\kappa_a & e^{idk_x}\kappa_a & e^{idk_b}k_y & e^{-idk_b}k_y & e^{id\kappa_b}\kappa_b & -e^{-id\kappa_b}\kappa_b \\
e^{iak_a}f_a & e^{-iak_a}f_a & -e^{ia\kappa_a}m_a & e^{-ia\kappa_a}m_a & -e^{iak_b}f_b & -e^{-iak_b}f_b & e^{ia\kappa_b}m_b & -e^{-ia\kappa_b}m_b \\
e^{idk_x}f_a & e^{idk_x}f_a & -e^{idk_x}m_a & e^{idk_x}m_a & -e^{idk_b}f_b & -e^{-ik_b}f_b & e^{id\kappa_b}m_b & -e^{-id\kappa_b}m_b \\
e^{iak_a}n_a & -e^{-iak_a}n_a & e^{ia\kappa_a}h_a & e^{-ia\kappa_a}h_a & -e^{iak_b}n_b & e^{-iak_b}n_b & -e^{ia\kappa_b}h_b & -e^{-ia\kappa_b}h_b \\
e^{idk_x}n_a & -e^{idk_x}n_a & e^{idk_x}h_a & e^{idk_x}h_a & -e^{idk_b}n_b & e^{-idk_b}n_b & -e^{id\kappa_b}h_b & -e^{-id\kappa_b}h_b
\end{pmatrix} = 0. \tag{A1}$$

Here, $k_{a,b} = \sqrt{k_{l(a,b)}^2 - k_y^2}$, $\kappa_{a,b} = \sqrt{k_{t(a,b)}^2 - k_y^2}$ are the $x$-components of the wave vector of the longitudinal and transverse mode in the layers and $k_y$ is the $y$-component of the wave vector. The dispersion relations for the modes in the media $a$ and $b$ are given by Eqs. (4) and (5). Other notations are defined as follows:

https://doi.org/10.1121/10.0024719

$$f_{a,b} = \frac{i}{\omega}(\rho_{a,b}\omega^2 + 2i\omega\eta_{a,b}k_y^2), \tag{A2}$$

$$m_{a,b} = 2\eta_{a,b}k_y\kappa_{a,b}, \quad n_{a,b} = 2\eta_{a,b}k_{a,b}k_y, \quad h_{a,b} = \eta_{a,b}(-k_y^2 + \kappa_{a,b}^2). \tag{A3}$$

## APPENDIX B: DISPERSION EQUATION WITH BULK DISSIPATION

Calculation of the determinant [Eq. (A1)] leads, after some simplifications mentioned in Sec. III D, to the dispersion Eq. (29). If the effects of dissipation in the bulk are not neglected, the parameters $\alpha$ and $\beta$ defined by Eq. (30) are replaced by the following formulas:

$$\begin{aligned}
\alpha_1 &= \frac{(\rho_b\omega^2 - 2\mu_b k_y^2)^2}{4k_b\kappa_b\mu_b^2}, \quad \alpha_2 = \frac{(\rho_a\omega^2 + 2i\omega\eta_a k_y^2)\rho_b\omega^2}{4k_a\kappa_b\mu_b^2},\\
\beta_0 &= \frac{k_y^2((\rho_a\omega^2 + i\omega\eta_a k_y^2)(\omega^2(\rho_a - \rho_b) + 2\mu_b k_y^2) + i\omega\eta_a k_y^2\rho_a\omega^2)\rho_b\omega^2}{8k_a k_b\kappa_b\mu_b^3},\\
\beta_1 &= \frac{\left[(\rho_a\omega^2 + 2i\omega\eta_a k_y^2)(\rho_a\omega^2 + \mu_b k_y^2) + \mu_b k_y^2\rho_a\omega^2\right](\rho_b\omega^2 - 2\mu_b k_y^2)\rho_b\omega^2}{16k_a k_b\kappa_b\mu_b^4},\\
\beta_2 &= \frac{\rho_a\rho_b\omega^4}{4k_b\mu_b^2}, \quad \beta_3 = \frac{(\rho_a\omega^2 + 2(\mu_b + i\omega\eta_a)k_y^2)(\rho_a\omega^2 + 2\mu_b k_y^2)}{4k_a\mu_b^2},\\
\beta_4 &= \frac{k_y^2(\omega^2(\rho_a - \rho_b) + 2(\mu_b + i\omega\eta_a)k_y^2)(\omega^2(\rho_a - \rho_b) + 2\mu_b k_y^2)}{4k_a k_b\kappa_b\mu_b^2},\\
\beta_5 &= \frac{k_y^2(\rho_b\omega^2 - 2\mu_b k_y^2)\left[(\rho_a\omega^2 + 2(\mu_b + i\omega\eta_a)k_y^2)(\omega^2(\rho_a - \rho_b) + 2\mu_b k_y^2) + i\omega\eta_a k_y^2\rho_b\omega^2\right]}{k_a k_b\kappa_b\mu_b^3}.
\end{aligned} \tag{B1}$$


[1]J. Ying and C. Yiling, "Application of elastic layered system in the design of road," Int. J. Eng. Res. Appl. **5**(Part 4), 82–85 (2015), available at https://www.ijera.com/papers/Vol5_issue7/Part%20-%204/O57048285.pdf.
[2]M. Ewing, W. Jardetsky, and F. Press, *Elastic Waves in Layered Media* (McGraw-Hill Book Co., New York, 1957).
[3]L. M. Brekhovskikh, *Waves in Layered Media* (Academic Press Inc., New York, 1960).
[4]S. M. Rytov, "Acoustical properties of a thinly laminated medium," Akust. Zh. **2**, 71 (1956) [Sov. Phys. Acoust. **2**, 68–80 (1956)].
[5]H. F. Cooper, Jr., "Reflection and transmission of oblique plane waves at plane interface between viscoelastic media," J. Acoust. Soc. Am. **42**, 1064–1069 (1967).
[6]R. P. Shaw and P. Bugl, "Transmission of plane waves through layered linear viscoelastic media," J. Acoust. Soc. Am. **46**, 649–654 (1969).
[7]M. I. Hussein, Erratum: "Theory of damped Bloch waves in elastic media," Phys. Rev. B **80**, 212301 (2009).
[8]R. P. Moiseyenko and V. Laude, "Material loss influence on the complex band structure and group velocity in phononic crystals," Phys. Rev. B **83**, 064301 (2011).
[9]C. L. Bacquet, H. Al Ba'ba'a, M. J. Frazier, M. Nouh, and M. I. Hussein, "Metadamping: Dissipation emergence in elastic metamaterials," Adv. Appl. Mech. **51**, 115–164 (2018).
[10]B. P. Konstantinov, "On the absorption of acoustic waves reflected from a solid boundary," Zh. Tekh. Fiz. **9**, 226–238 (1939).
[11]H. Heo, E. Walker, Y. Zubov, D. Shymkiv, D. Wages, A. Krokhin, T.-Y. Choi, and A. Neogi, "Non-reciprocal acoustics in a viscous environment," Proc. R. Soc. A **476**, 20200657 (2020).
[12]J. W. S. Rayleigh, *The Theory of Sound*, 2nd ed. (Macmillan and Co., New York, 1896), Chap. XIX, Sec. 345.
[13]A. K. Chopra, *Dynamics of Structures*, 2nd ed. (Prentice-Hall, Englewood Cliffs, NJ, 2001).
[14]M. D. Guild, V. M. García-Chocano, W. Kan, and J. Sánchez-Dehesa, "Acoustic metamaterial absorbers based on multilayered sonic crystals," J. Appl. Phys. **117**, 114902 (2015).
[15]B. Djafari-Rouhani and L. Dobrzynski, "Vibrational contribution to the surface specific heat of a fluid," J. Phys. France **43**, 523–529 (1982).
[16]C. J. T. Sewell, "The extinction of sound in a viscous atmosphere by small obstacles of cylindrical and spherical form," Proc. R. Soc. London A **83**, 547–548 (1910).
[17]S. H. Lamb, *Hydrodynamics*, 6th ed. (Dover, New York, 1945).
[18]W. H. Lin and A. C. Raptis, "Acoustic scattering by elastic solid cylinders and spheres in viscous fluids," J. Acoust. Soc. Am. **73**, 736–748 (1983).
[19]A. D. Pierce, *Acoustics: An Introduction to Its Physical Principles and Applications* (Acoustical Society of America, New York, 1989).
[20]B. Sprik and G. H. Wegdam, "Acoustic band gaps in composites of solids and viscous liquids," Solid State Commun. **106**, 77–81 (1998).
[21]X. Zhang, Z. Liu, J. Mei, and Y. Liu, "Acoustic band gaps for a two-dimensional periodic array of solid cylinders in viscous liquid," J. Phys.: Condens. Matter **15**, 8207–8212 (2003).
[22]E. Reyes-Ayona, D. Torrent, and J. Sánchez-Dehesa, "Homogenization theory for periodic distributions of elastic cylinders embedded in a viscous fluid," J. Acoust. Soc. Am. **132**, 2896–2908 (2012).
[23]M. Ibarias, Y. Zubov, J. Arriaga, and A. A. Krokhin, "Phononic crystal as a homogeneous viscous metamaterial," Phys. Rev. Res. **2**, 022053(R) (2020).
[24]M. Ibarias, J. Doporto, A. A. Krokhin, and J. Arriaga, "Tuning the decay of sound in a viscous metamaterial," Philos. Trans. R. Soc. A **380**, 20220007 (2022).
[25]V. S. J. Craig, C. Neto, and D. R. M. Williams, "Shear-dependent boundary slip in an aqueous Newtonian liquid," Phys. Rev. Lett. **87**, 054504 (2001).
[26]Y. Zhu and S. Granick, "Viscosity of interfacial water," Phys. Rev. Lett. **87**, 096104 (2001).

[27]T. Becker and F. Mugele, "Nanofluidics: Viscous dissipation in layered liquid films," Phys. Rev. Lett. **91**, 166104 (2003).
[28]A. B. Pippard, "The anomalous skin effect in normal metals," Proc. R. Soc. A **191**, 385–399 (1947).
[29]G. E. H. Reuter and E. H. Sondheimer, "The theory of anomalous skin effect in metals," Proc. R. Soc. A **195**, 336–364 (1948).
[30]J. D. Jackson, *Classical Electrodynamics*, 3rd ed. (Wiley, New York, 1998), p. 298.
[31]A. N. Norris, "An inequality for longitudinal and transverse wave attenuation coefficients," J. Acoust. Soc. Am. **141**, 475–479 (2017).
[32]Y. El Hassouani, E. H. El Boudouti, B. Djafari-Rouhani, and H. Aynaou, "Sagittal acoustic waves in finite solid-fluid superlattices: Band-gap structure, surface and confined modes, and omnidirectional reflection and selective transmission," Phys. Rev. B **78**, 174306 (2008).
[33]I. Quotane, E. Houssaine, E. H. Boudouti, and B. Djafari-Rouhani, "Trapped mode-induced Fano resonance and acoustical transparency in a one-dimensional solid–fluid phononic crystal," Phys. Rev. B **97**, 024304 (2018).
[34]Y. Zubov, B. Djafari-Rouhani, Y. Jin, M. Sofield, E. Walker, A. Neogi, and A. Krokhin, "Long-range nonspreading propagation of sound beam through periodic layered structure," Commun. Phys. **3**, 155–163 (2020).
[35]G. Borrmann, "Über extinktionsdiagramme der röntgenstrahlen von quarz" ("About extinction diagrams of the x-rays of quartz"), Phys. Z **42**, 157–162 (1941).
[36]M. V. Bogdanova, Yu. E. Lozovik, and S. L. Eiderman, "An optical analog of the Borrmann effect in photonic crystals," J. Exp. Theor. Phys. **110**, 604–612 (2010).
[37]V. Novikov and T. Murzina, "Borrmann effect in photonic crystals," Opt. Lett. **42**, 1389–1392 (2017).
[38]A. Cebrecos, R. Picó, V. Romero-García, A. Yasser, L. Maigyte, R. Herrero, M. Botey, V. J. Sánchez-Morcillo, and K. Staliunas, "Enhanced transmission band in periodic media with loss modulation," Appl. Phys. Lett. **105**, 204104 (2014).
[39]A. Coutant, Y. Aurégan, and V. Pagneux, "Anomalous transmission through periodic resistive sheets," J. Acoust. Soc. Am. **147**, 3124–3135 (2020).
[40]S. Yang, J. H. Page, Z. Liu, M. L. Cowan, C. T. Chan, and P. Sheng, "Ultrasound tunneling through 3D phononic crystals," Phys. Rev. Lett. **88**, 104301 (2002).
[41]V. Laude, J. M. Escalante, and A. Martínez, "Effect of loss on the dispersion relation of photonic and phononic crystals," Phys. Rev. B **88**, 224302 (2013).
[42]M. D. Guild, V. M. Garcia-Chocano, W. Kan, and J. Sánchez-Dehesa, "Enhanced inertia from lossy effective fluids using multi-scale sonic crystals," AIP Adv. **4**, 124302 (2014).
[43]I. E. Psarobas, "Viscoelastic response of sonic band-gap materials," Phys. Rev. B **64**, 012303 (2001).
[44]X. Li, M. Zhao, X. Yu, J. W. Chua, Y. Yang, K. M. Lim, and W. Zhai, "Multifunctional and customizable lattice structures for simultaneous sound insulation and structural applications," Mater. Des. **234**, 112354 (2023).
[45]T. Qu, B. Wang, and H. Min, "Lightweight composite partitions with high sound insulation in hotel interior spaces: Design and application," Build. **12**, 2184 (2022).